RSC Advances

ROYAL SOCIETY OF CHEMISTRY

www.rsc.org/advances

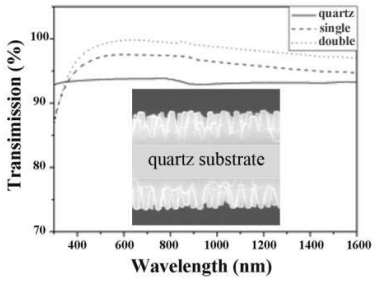

A simple method was presented to increase the transmission by preparing multiscale tapered pillars on both surfaces of quartz slides.

Cite this: DOI: 10.1039/c0xx00000x

www.rsc.org/xxxxxx

ARTICLE TYPE

Fabrication of Biomimetic Patterns for High Transmission and Antifogging Property†

Hongbo Xu‡, Lingxiao Liu‡, Feifei Wu, Daren Xu and Nan Lu*

Received (in XXX, XXX) Xth XXXXXXXXX 20XX, Accepted Xth XXXXXXXXX 20XX

DOI: 10.1039/b000000x

Enhancing the transmission of optical components is important for improving the performance of optical and optoelectronic devices such as photovoltaic panels and concentration photovoltaic system. A simple method to enhance the transmission of quartz slides is presented here by fabricating multiscale tapered pillars on both sides of quartz slides. The multiscale tapered nanopillars, which introduced refractive index gradient on both surfaces, were created by reactive ion etching with dewetted Ag thin films as masks. The presence of the gradient on both surfaces greatly reduces the loss of light caused by reflection, which will enhance the total transmission light. Excellent transmission over the visible and near infrared region is achieved after optimizing the parameter of structure. The transmission of the dual-sided structured quartz is enhanced to higher than 99% over the wavelengths from 650 to 850 nm. Meanwhile, the structured quartz exhibits antifogging property which is needed in optical and optoelectronic devices.

1. Introduction

Optical devices and many energy-related applications rely on quartz as a protecting barrier from fogging and as a transparent window for light propagation.[1-3] However, the transmission through a quartz window is limited by the naturally occurring Fresnel reflection, always present at any interface separating different indices of refraction (n). Standard quartz typically reflects 8% of the incoming light at a normal angle of incidence, and this percentage is even increased at higher incidence angles. Therefore, achieving higher optical transmission in the visible and near-IR spectra by an effective antireflection (AR) coating is a key issue for overcoming some important obstacles for optoelectronic devices, such as the losses due to the surface reflection, the angular dependence of the reflectivity for the standard multilayer coatings in PV panels and CPV systems, poor light extraction efficiency in light-emitting diodes, poor contrast and brightness in display devices.[4-8]

Up to now, two main approaches have been applied to fabricate efficient AR coatings: thin film coatings and graded index coatings.[9] The limitation of thin film coatings is that high transmission can be achieved only in narrow ranges of wavelength and incidence angles.[8] The problems of stability induced by adhesiveness and thermal mismatch are often associated with that approach. The latter approach is the manufacturing of the so called graded index coatings, where n is gradually varied from quartz to air by the gradual variation of composition of a single layer material.[10-15] This is hard to be realized because n for a solid material like quartz (～1.5) is significantly different from that of air (～1). Observations on the corneas of nocturnal moths indicate that surface-relief arrays with dimension smaller than the wavelength of incident light can be an alternative to thin film coatings, which are more stable and durable than surface coatings since only one material is involved.[16] In the last decade, increasing efforts have been given to the fabrication of sub-wavelength structures （SWS） for enhancing transmission. SWS are usually fabricated by taking etching process with shadow masks.[17-22] Some techniques have been proposed to generate shadow masks such as electron-beam lithography, laser interference lithography, and nanoimprint lithography.[12, 23-28] These techniques are restricted from practical applications due to the expensive equipments and complicated procedures.[9, 13, 29] Self-assembled colloidal nanospheres and anodic porous alumina membrane combined with reactive ion etching (RIE) process have been used for fabricating periodic upright tapered SWS.[30, 31] These tapered structures with high aspect ratio can enhance transmission over a wide range of wavelengths from visible to near-infrared range.[19, 32, 33] Although both sides of quartz substrate can reflect visible light, most studies on transmission enhancement are focused on fabricating SWS on one side of the transparent substrate.[29] The incident light gets into the substrates and a part of light will be reflected back at the substrate/air interface especially under oblique incidence.[34, 35] This part of the light loss will cause the reduction of the transmission. So it is crucial to introduce antireflection layer on both sides of transparent substrates for increasing transmission. Therefore, both sides of a quartz substrate need fabricate SWS for higher transmission.[3, 9]

It is known that SWS with certain scale can only maximize light transmission for short range of wavelengths, so SWS with multiscale are needed to enhance light transmission at wide range of wavelengths. Surfaces with micro- and nanometer scale composite structures were fabricated for suppressing reflection in our previous work.[12, 16, 25] However, less attention has been paid on enhancing the transmission property at the visible range, and the fabrication process could be further simplified. The metal nanoparticles formed by a thermal dewetting process are ideal etching masks for fabricating multiscale SWS.[13, 36, 37] Meanwhile, the size of SWS can be easily adjusted by tuning the thickness of

thin films.[13, 37] According to Rayleigh, the enhancement of transmission depends on the parameter of SWS.[38] By tuning the parameter of SWS, to enhance the transmission at the full visible range can be made easily.[13] Therefore, multiscale SWS can be fabricated with the nanoparticles as etching mask, which can maximize light transmission at a wide range of wavelengths.

Simultaneously, Overall enhancing transmission is a function of AR-layer thickness d and wavelength λ. Therefore, the size and height of sub-wavelength structure should follow the following principles: (1) To avoid scattering from the optical interface, the lateral dimension of the SWS has to be smaller than the wavelength of the incoming light ("lower wavelength limit P< λ/n", where P is the period of SWS); (2) For a graded-index transition, substantial antireflection is obtained when the value of d/λ is about 0.4. For enhancing transmission at visible light, the lateral sizes of SWS should be smaller than 260 nm, and the heights of SWS should be greater than 300 nm.[16, 25]

Herein, we proposed an efficient method to enhance the transmission of quartz substrates by fabricating multiscale nanopillars on both sides of quartz substrates. For high transmission over visible light, the periods and heights of the fabricated multiscale tapered nanopillars are smaller than 200 nm and higher than 340 nm respectively. The multiscale SWS were fabricated by reactive ion etching with dewetting Ag thin films as masks. The total transmission was dramatically increased over the full visible and near infrared range with an incidence angle up to 50°. Moreover, the multiscale SWS exhibit excellent antifogging properties, which are important in optical and optoelectronic devices.

2. Experimental Section

2.1 Chemicals and Materials. The Ag sheet (99.999%) was purchased from Sigma Aldrich Co. The quartz slices were obtained from Beijing Zhongjingkeyi Technology Company, China. Analytical reagent-grade ethanol, acetone, chloroform, HNO_3 solution were purchased from commercial sources and used without further purification.

2.2 Fabrication of metal thin film. The quartz slices ($3 \times 3\ cm^2$) were treated with oxygen Plasma System (100, PVA Tepla) at 300 W, 660 mTorr for 3 min and thoroughly cleaned with acetone, chloroform and ethanol in an ultrasonic bath for 5 mins respectively. Ag films were evaporated on the quartz substrates using a thermal evaporation system (Shenyang Keyou Co.). The working pressure was 5.0×10^{-4} pa, the evaporation rate was 1 nm/min with the applied current of 35 A.

2.3 Dewetting of metal thin film. A thermal dewetting process was introduced to form metal nanoparticles. The samples were put into a muffle furnace in nitrogen protection at the temperature of 300℃ and kept for 15 mins. The metal film shrank into nanoparticles to stay at the minimum surface energy state.[34]

2.4 The formation of multiscale nanopillars. RIE was carried out on a Plasmalab Oxford 80 plus (ICP 65) system (Oxford Instrument Co. UK) with the Ag nanoparticles as mask. The processing gases were CHF_3 (30 sccm) and Ar (15 sccm), with the RF power and the chamber pressure at 100 W and 30 mTorr, respectively. After that, the residual Ag was removed by immersing the sample into 10% HNO_3 solution.

2.5 Formation of dual-sided nanostructures. To fabricate multiscale pillars on both sides of quartz, silver film was evaporated on the back side of quartz substrate with pillars, and then dewetting and RIE process were co nducted as described in 2.2, 2.3 and 2.4.

2.6 Characterization. Scanning electron microscope (SEM) images were taken on JEOL JSM 6700F field emission SEM with primary electron energy of 3 kV, and the samples were sputtered with a layer of Au (ca. 2 nm thick) to improve conductivity prior to imaging. The spectra were collected on a spectroscopy meter (Shimadzu UV3600, Shimadzu, Japan). The contact angle was measured with the commercial contact angle system (DataPhysics, OCA 20).

Results and Discussion

The fabrication procedure is schematically shown in Figure 1. The fabrication details can be seen in Experimental Section 2.2 to 2.5.

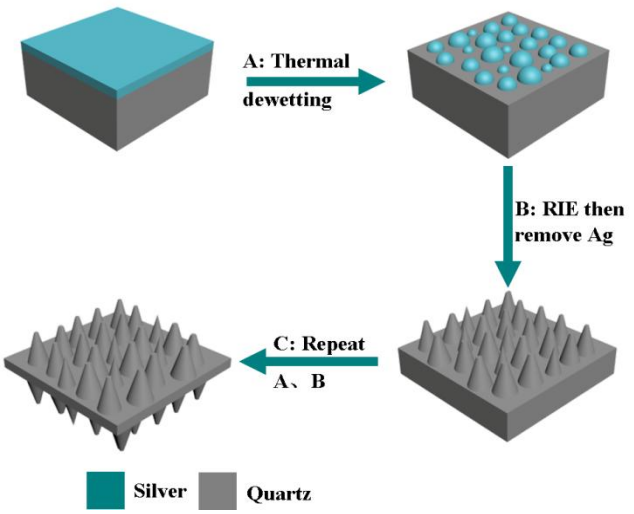

Figure 1. Schematic illustration of the fabrication process. (A) Ag nanoparticles are formed by thermal dewetting. (B) Tapered nanopillars are created by taking RIE process with Ag nanoparticles as mask, and removing the residual Ag by inserting the sample to 10% HNO_3. (C) Repeat the fabrication process on the back side of substrate.

To investigate the effect of the film thickness on the size of formed Ag nanoparticles, 7, 13 and 20 nm silver were initially evaporated respectively. The SEM of Ag films can be seen in Figure S1. Ag islands were formed at the beginning of evaporation, which link together with the increase of film thickness. Then according to the thermal dewetting method by Lee,[35] the substrate was kept at 300 ℃ for 15 min in a muffle furnace to induce rapid thermal dewetting of the deposited Ag film, which occurs due to the increased surface energy in the metal film by heating.[39, 40] The dewetting results are shown in Figure 2A–C.

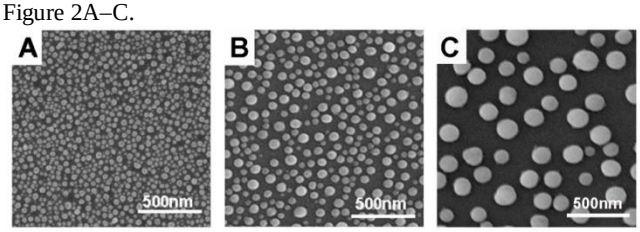

Figure 2. SEM images of the Ag nanoparticles formed by Ag film of different thicknesses. (A) 7 nm, (B) 13 nm and (C) 20 nm.

Figure 2A shows that the dimensions of the Ag nanoparticles range from 20 to 50 nm, with an average distance less than 40 nm. When the thickness is 13 nm, the dimensions of the Ag nanoparticles range from 50 to 100 nm, with an average distance less than 90 nm, as presented in Figure 2B. When the thickness is 20 nm, the dimensions of the Ag nanoparticles range from 100 to 150 nm, with an average distance less than 150 nm, as shown in Figure 2C. The size of the nanoparticles increases with increasing film thickness, while the density decreases when the film thickness increases. The detailed statistics of dimensions of Ag nanoparticles made by Ag films of different thickness can be seen in Table 1 (supporting information).

According to Rayleigh, the reflectance of SWS depends on the effective thickness (h) which equals to the height of nanopillars and spacing (s) of the arrays, and on the wavelength (λ) of the light at normal incidence.[37, 41] Ultralow reflectance occurs when $s<\lambda<2.5h$ which means the transmission of SWS is greatly enhanced. The highest transmission can be obtained at $\lambda>np$ with normal incidence and $\lambda> 2np$ with oblique incidence,[42, 43] where n is refractive index of substrates and p is for the period of nanostructures. For the vision applications, the feature sizes of SWS must be smaller than 260 nm. The feature sizes of SWS obtained with thermal dewetting 13 nm Ag film as etching mask were smaller than 260 nm, and these SWS achieved the highest transmission at visible range. Therefore, 13 nm Ag film is chosen for forming etching mask to achieve the best transmission enhancing property at visible range. After the fabrication of dual-sided SWS by thermal dewetting and RIE, the residual Ag was removed using 10% HNO_3 solution. The SEM images of SWS were taken and shown in Figure 3.

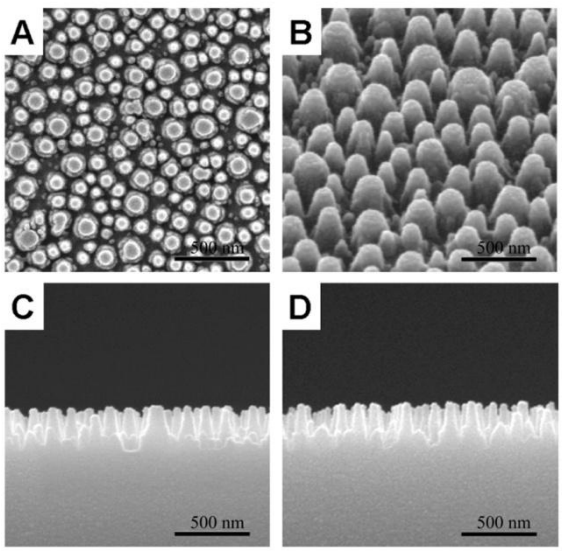

Figure 3. (A), (B) Top view and 45 ° tilt view SEM images of the top side structures; (C), (D) cross-sectional SEM images of the structures on top and the bottom, respectively.

Figure 3A shows that the average distance of the tapered nanopillars is same as that of the etching mask. The multiscale SWS can be observed in the 45 ° titled SEM image, as shown in Figure 3B. The calculated etching ratio of quartz to Ag nanoparticles in this process is about 15-20:1. That is why multiscale SWS can be fabricated with this method. Figure 3C reveals that the height of tapered nanopillars is around 340 nm, and the average spacing between the pillars is 120 nm. The average spacing ranges from 78 nm to 183 nm. Figure 3D shows the multiscale SWS fabricated on the other side of the quartz slide, which is almost same as SWS on the first side.

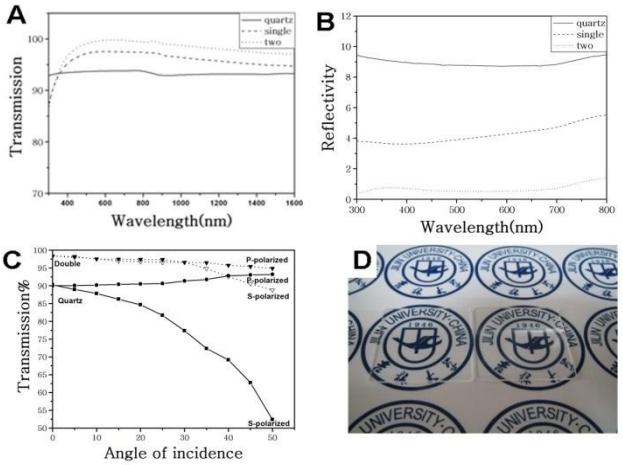

Figure 4. Comparison of the transmission (A) and specular reflection (B) for a planar quartz substrate (solid line), single-sided (dashed line) and dual-sided structured quartz (dotted line). (C) Angle dependent transmission of the planar quartz and dual-sided structured slide. (D) Digital photographs of the structured slide (left) and planar quartz slide (right).

Transmission and reflection of the quartz slides with one side SWS, dual-sided SWS and planar are given in Figure 4A and Figure 4B respectively. Figure 4A shows that the transmission of the quartz slide with dual-sided SWS (the dotted line) is higher than that of planar quartz slide (the solid line) and the single-sided one (the dashed line). The average transmission of the dual-sided SWS is above 99% from 650 nm to 850 nm. The maximum transmission of 99.5% at 780 nm indicates that the light can go through the sample with only a little loss. The transmission performance of structured quartz slides is worse than that of planar quartz slide at the wavelength from 350 nm to 365 nm. This is due to light absorption caused by the nanostructures. However, transmission and reflectance play a major role when $\lambda>400$ nm.[44] The high transmission is due to the ultralow reflectance. The specular reflection was measured at an incidence angle of 5 °. As shown in Figure 4B, the reflectance of the dual-sided structured sample is below 1.5% (the dotted line) over the whole visible spectrum, while that of the single-sided structured one is less than 5% (the dashed line), and that of the reflectance of planar quartz substrate is around 10% (the solid line). This indicates that the reflection from the back side interface is depressed. The transmission is enhanced not only at the air/substrate interface but also at the substrate/air interface. The lowest average reflectance (~0.8%) can be obtained at the range of 450 nm to 700 nm on the dual-sided structured sample, which nearly covered the whole visible spectrum. Figure 4C shows the angle-dependent transmission of the planar quartz and dual-sided structured surfaces. It was measured with He–Ne laser (632.8 nm) at AOI from 0 ° to 50 ° for p- and s- polarization, where p and s denote planes of incidence parallel and perpendicular to the

electrical field of the light waves, respectively. The performance of the structured quartz is better than that of the planar quartz for both p- and s- polarized light. For both p- and s- polarization, the transmission of the dual-sided structured sample reaches a value of 99.2% when the AOI is 30°. The photograph of a planar quartz substrate and dual-sided structured sample is shown in Figure 4D. The dual-sided structured sample (the left one: 3 × 3 cm^2) displays a higher transmission than the planar quartz (the right one).

This method is also suitable for curved substrates. We fabricated SWS on both sides of the planconvex lens with diameter of 30 mm, focal length of 100 mm and curvature radius of 49.8 mm. The transmission of the dual-sided structured planconvex lens was enhanced in the visible light region, see Figure S2. It can be observed that the dual-sided structured planconvex lens (left) exhibits higher transmission and lower reflection than the one without nanostructures (right).

The wetting property of the surface can be enhanced by nanostructures due to the quartz surface is intrinsic hydrophilic.[45] This will bring antifogging property to substrate which is desired in the optical devices. The water wetting behavior of the SWS surfaces was evaluated by water contact angle measurement with a water droplet of 5 μL.

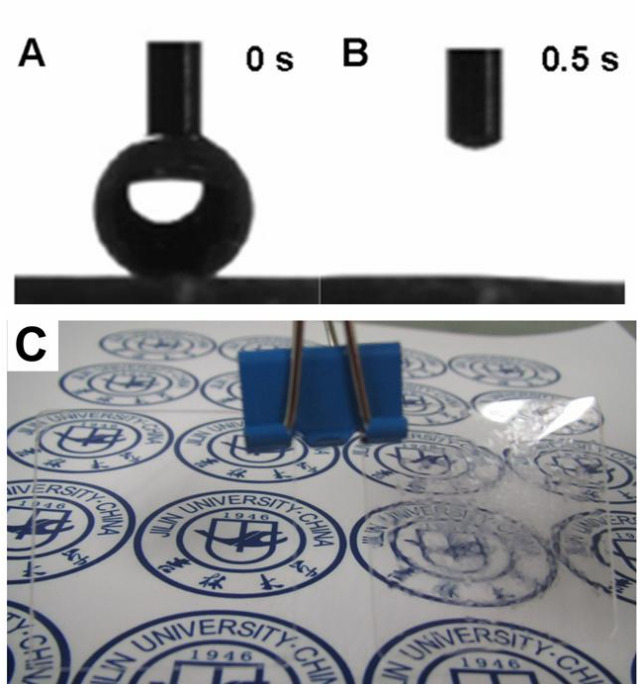

Figure 5. (A), (B) Contact angle measurements for a water droplet (5 μL) on structured surfaces. (C) Digital photographs of a dual-sided structured slide (left) and a planar quartz slide (right) taken from a refrigerator (-5 ℃) to humid air (ca. 50% RH, 20 ℃).

As shown in Figure 5A and 5B, the water droplet spreads over the surface within 0.5 s, which means the surface is superhydrophilic. A 20° water contact angle of quartz substrate is reported elsewhere.[8] According to Wenzel's equation: $\cos\theta_a = r\cos\theta$, where r is the roughness of surface, θ_a is the contact angle of structured surface, θ is the contact angle of quartz substrate.[46-48] The surface structuring increases the roughness of surface. So the nanostructures obviously increase the wettability of substrates. Superhydrophilic surfaces have antifogging property because the condensed water droplets will spread at the surface instantaneously to avoid the formation of water droplets. The antifogging behavior of structured surfaces is demonstrated. A planar slide and a double-sided SWS slide were both cooled to about -5 ℃ in a refrigerator, and then both slides were instantaneously exposed to the humid air (ca. 50 % RH, 20 ℃). Figure 5C shows the visible difference between the two slides clearly. After exposure to humid air, the transparence of the structured slide (left) is higher than that of the planar slide (right).

Conclusions

We have presented an efficient method to enhance transmission of transparent substrates by creating multiscale tapered nanopillar arrays on both sides of substrate. The multiscale SWS allows for enhancing transmission at wide range. The structure size can be optimized by simply changing the thickness of silver film to achieve an ultrahigh transmission at the whole visible and near infrared region. Furthermore, the structured substrates exhibit excellent antifogging behaviour. This method provides a facile approach for producing high transmission on large scale with low cost and high throughput, which may be utilized in optical and optoelectronic fields to improve the performance of photon sensitive devices.

Acknowledgments

H.B. Xu. and L.X. Liu contributed equally to this work. This work was supported by the National Natural Science Foundation of China (21273092 and 20373019).

Notes and references

Address, State Key Laboratory of Supramolecular Structure and Materials, College of Chemistry, Jilin University, Changchun 130012, P. R. China

Fax: (+86)-431-85168477; Tel: (+86)-431-85168477; E-mail: luenan@jlu.edu.cn

† Electronic Supplementary Information (ESI) available: Details of Ag nanoparticles formed by thermal dewetting, SEM images of the deposited Ag films of different thicknesses, Photographs of the dual-sided structured lens and plan convex lens are given in Supporting Information. See DOI: 10.1039/b000000x/

‡ These two authors contributed equally to this article.

Reference

1. C. B. Song, Y. H. Qiang, Y. L. Zhao, X. Q. Gu, D. M. Song and L. Zhu, *Appl. Surf. Sci.*, 2014, **305**, 792-796.
2. P. Prepelita, V. Craciun, G. Sbarcea and F. Garoi, *Appl. Surf. Sci.*, 2014, **306**, 47-51.
3. S. Ji, J. Park and H. Lim, *Nanoscale*, 2012, **4**, 4603-4610.
4. Y. R. Jung, Y. W. Jung and K.-S. Sohn, *J. Electrochem. Soc.*, 2009, **156**, J321-J325.
5. P. Blake, P. D. Brimicombe, R. R. Nair, T. J. Booth, D. Jiang, F. Schedin, L. A. Ponomarenko, S. V. Morozov, H. F. Gleeson, E. W. Hill, A. K. Geim and K. S. Novoselov, *Nano Lett.*, 2008, **8**, 1704-1708.
6. R. L. Hoffman, B. J. Norris and J. F. Wager, *Appl. Phys. Lett.*, 2003, **82**, 733-735.
7. Y. F. Li, F. Li, J. H. Zhang, C. L. Wang, S. J. Zhu, H. J. Yu, Z. H. Wang and B. Yang, *Appl. Phys. Lett.*, 2010, **96**,153305.

8. J. Hiller, J. D. Mendelsohn and M. F. Rubner, *Nat. Mater.*, 2002, **1**, 59-63.
9. Y. Li, J. Zhang, S. Zhu, H. Dong, F. Jia, Z. Wang, Z. Sun, L. Zhang, Y. Li, H. Li, W. Xu and B. Yang, *Adv. Mater.*, 2009, **21**, 4731-4734.
10. X. Li and Y. C. Han, *J. Mater. Chem.*, 2011, **21**, 18024-18033.
11. F. J. Garcia-Vidal, L. Martin-Moreno, T. W. Ebbesen and L. Kuipers, *Rev. Mod. Phys.*, 2010, **82**, 729-787.
12. H. Xu, N. Lu, G. Shi, D. Qi, B. Yang, H. Li, W. Xu and L. Chi, *Langmuir*, 2011, **27**, 4963-4967.
13. D. Infante, K. W. Koch, P. Mazumder, L. Tian, A. Carrilero, D. Tulli, D. Baker and V. Pruneri, *Nano Res.*, 2013, **6**, 429-440.
14. S.-Y. Chuang, H.-L. Chen, J. Shieh, C.-H. Lin, C.-C. Cheng, H.-W. Liu and C.-C. Yu, *Nanoscale*, 2010, **2**, 799-805.
15. J. W. Leem, Y. M. Song and J. S. Yu, *Nanoscale*, 2013, **5**, 10455-10460.
16. Y. Wang, N. Lu, H. Xu, G. Shi, M. Xu, X. Lin, H. Li, W. Wang, D. Qi, Y. Lu and L. Chi, *Nano Res.*, 2010, **3**, 520-527.
17. K. C. Camargo, A. F. Michels, F. S. Rodembusch and F. Horowitz, *Chem Commun (Camb)*, 2012, **48**, 4992-4994.
18. Y. Li, J. Zhang and B. Yang, *Nano Today*, 2010, **5**, 117-127.
19. S. Chattopadhyay, Y. F. Huang, Y. J. Jen, A. Ganguly, K. H. Chen and L. C. Chen, *Mater. Sci. Eng.: R: Reports*, 2010, **69**, 1-35.
20. Y. Ono, Y. Kimura, Y. Ohta and N. Nishida, *Appl. Optics*, 1987, **26**, 1142-1146.
21. B. Weng, J. Qiu, Z. Yuan, P. R. Larson, G. W. Strout and Z. Shi, *Appl. Phys. Lett.*, 2014, **104**, 021109.
22. Y. M. Song, Y. Jeong, C. I. Yeo and Y. T. Lee, *Opt. Express*, 2012, **20**, A916-A923.
23. Y. Kanamori, E. Roy and Y. Chen, *Microelectron. Eng.*, 2005, **78-79**, 287-293.
24. J. Xu, Z. Wang, Z. Zhang, D. Wang and Z. Weng, *J. Appl. Phys.*, 2014, **115**.
25. F. Wu, G. Shi, H. Xu, L. Liu, Y. Wang, D. Qi and N. Lu, *ACS Appl. Mater. Interfaces*, 2013, **5**, 12799-12803.
26. Y. Luo, C. Wang, L. Wang, Y. Ding, L. Li, B. Wei and J. Zhang, *ACS Appl. Mater. Interfaces*, 2014, **6**, 10213-10219.
27. Y.-Q. Li, B. Zhu, Y. Li, W. R. Leow, R. Goh, B. Ma, E. Fong, M. Tang and X. Chen, *Angew. Chem., Int. Ed.*, 2014, **53**, 5837-5841.
28. J. Martinez-Perdiguero, A. Retolaza, A. Juarros, D. Otaduy and S. Merino, *26th European Conference on Solid-State Transducers, Eurosensor 2012*, 2012, **47**, 805-808.
29. J. W. Leem, Y. Yeh and J. S. Yu, *Opt. Express*, 2012, **20**, 4056-4066.
30. T. Yanagishita, M. Masui, N. Ikegawa and H. Masuda, *J. Vac. Sci. Technol., B*, 2014, **32**, 021809.
31. J. Chen, B. Wang, Y. Yang, Y. Shi, G. Xu and P. Cui, *Appl. Optics*, 2012, **51**, 6839-6843.
32. Y.-R. Lin, K. Y. Lai, H.-P. Wang and J.-H. He, *Nanoscale*, 2010, **2**, 2765-2768.
33. H. K. Raut, S. S. Dinachali, Y. C. Loke, R. Ganesan, K. K. Ansah-Antwi, A. Gora, E. H. Khoo, V. A. Ganesh, M. S. Saifullah and S. Ramakrishna, *ACS Nano*, 2015, **9**, 1305-1314.
34. Y. M. Park, B. H. Kim and Y. H. Seo, *Micro Nano Lett.*, 2013, **8**, 460-464.
35. Y. Lee, K. Koh, H. Na, K. Kim, J.-J. Kang and J. Kim, *Nanoscale Res. Lett.*, 2009, **4**, 364-370.
36. L. Rayleigh, *Proc. London Math. Soc.*, 1879, **S1-11**, 51-56.
37. E. Hein, D. Fox and H. Fouckhardt, in *Nanoengineering: Fabrication, Properties, Optics, and Devices Vii*, eds. E. A. Dobisz and L. A. Eldada, 2010, vol. 7764.
38. Y. J. Oh, J. J. Kim and K. H. Jeong, *Small*, 2014, **10**, 2558-2563.
39. J.-M. Lee and B.-I. Kim, *Mater. Sci. Eng.: A*, 2007, **449**, 769-773.
40. A. Schleunitz, C. Spreu, J. Lee and H. Schift, *J. Vac. Sci. Technol., B*, 2010, **28**, C6m41-C46m44.
41. C. C. Striemer and P. M. Fauchet, *Appl. Phys. Lett.*, 2002, **81**, 2980-2982.
42. P. B. Clapham and M. C. Hutley, *Nature*, 1973, **244**, 281-282.
43. W. H. Southwell, *Opt. Lett.*, 1983, **8**, 584-586.
44. T. J. Suleski, M. Schulze, H. J. Fuchs, E. B. Kley, A. Tünnermann, W. V. Schoenfeld and J. J. Wang, *Proc. of SPIE*, 2008, **6883**, 68830N-68830N-68810.
45. F. C. Cebeci, Z. Wu, L. Zhai, R. E. Cohen and M. F. Rubner, *Langmuir*, 2006, **22**, 2856-2862.
46. R. N. Wenzel, *Ind. Eng. Chem.*, 1936, **28**, 988-994.
47. J. A. Howarter and J. P. Youngblood, *Macromol. Rapid Commun.*, 2008, **29**, 455-466.
48. K. Liu, X. Yao and L. Jiang, *Chem. Soc. Rev.*, 2010, **39**, 3240-3255.